Lihua Jin
School of Engineering and Applied Sciences,
Kavli Institute for Nanobio Science
and Technology,
Harvard University,
Cambridge, MA 02138

Anesia Auguste
Department of Polymer Science and Engineering,
University of Massachusetts,
Amherst, MA 01003

Ryan C. Hayward[1]
Department of Polymer Science and Engineering,
University of Massachusetts,
Amherst, MA 01003
e-mail: hayward@umass.edu

Zhigang Suo[1]
School of Engineering and Applied Sciences,
Kavli Institute for Nanobio Science
and Technology,
Harvard University,
Cambridge, MA 02138
e-mail: suo@seas.harvard.edu

Bifurcation Diagrams for the Formation of Wrinkles or Creases in Soft Bilayers

Subject to compression, elastic materials may undergo bifurcation of various kinds. A homogeneous material forms creases, whereas a bilayer consisting of a stiff film and a compliant substrate forms wrinkles. Here, we show several new types of bifurcation behavior for bilayers consisting of films and substrates of comparable elastic moduli. Depending on the ratios of moduli and thicknesses of the two materials, the critical strain for the onset of creases can be either smaller or larger than that for the onset of wrinkles. When the critical strain for the onset of creases is lower than that of wrinkles, creases can be subcritical or supercritical. When the critical strain for the onset of wrinkles is lower than that of creases, wrinkles can further channel to creases at a strain much lower than the critical strain for the onset of creases in a homogeneous material. Experiments, conducted with bilayer polydimethylsiloxane (PDMS) structures subject to compressive loading, show that the different types of bifurcation behavior agree with the theoretical predictions. [DOI: 10.1115/1.4030384]

Keywords: mechanical instability, creases, wrinkles, bilayer, bifurcation

1 Introduction

Soft materials, such as elastomers, gels, and living tissues, are often under compression due to forces, swelling, or growth. When the compression exceeds some critical strain, the soft materials undergo elastic instability, forming, e.g., wrinkles or creases [1–3]. Elastic instability of various kinds has been used in engineering to fabricate stretchable electronics [4], measure material properties [5], tune adhesion [6,7], change wettability [8], and control surface chemistry [9]. Wrinkles and creases also provide forms and functions in nature, such as formation of fingerprints [10], invagination of embryos [11], development of guts [12], folding of brains [13–15], and morphogenesis of viruses [16] and plants [17–24].

Wrinkles and creases are two distinct types of instability [25]. Wrinkles deviate from the flat state by a field of infinitesimal strain in a finite region, whereas a crease deviates from the flat state by a field of large strain in an infinitesimal region (Fig. 1). To determine the critical strain for the onset of wrinkles, a field of infinitesimal strain is superimposed upon the flat state [26–29]. This superimposed field linearizes the field equations around the flat state of finite deformation, leading to an eigenvalue problem. By contrast, the critical strain for the onset of a crease cannot be determined by linearization around the flat state, but can be determined by allowing the surface to form a localized region of self-contact.

Engineering systems and living tissues often involve layered materials of dissimilar elastic moduli [12,13,15,30–32]. Several special cases have been well studied. For a stiff thin film on a compliant thick substrate, the critical strain for the onset of wrinkles is smaller than that for the onset of creases, and wrinkles are observed in experiments [1–3,33,34]. For a homogeneous material, the critical strain for the onset of wrinkles is larger than that for the onset of creases, and creases are observed in experiments [25,35–42]. For layered materials of comparable thicknesses and moduli, the critical strain for the onset of wrinkles can be either smaller or larger than that for the onset of creases [43–47]. It is tempting to expect a layered material to form wrinkles if the critical strain for the onset of wrinkles is smaller than that for the onset of creases, or vice versa.

This expectation turns out to be wrong. In many cases, the bifurcation points themselves do *not* predict the behavior of a layered material. Rather, we need to construct bifurcation diagrams. In a bifurcation diagram, one axis represents the load (e.g., the compressive strain in this paper), and the other axis represents the state of the system using a parameter (e.g., the depth of crease or the energy of the system). As the load changes, the system goes through a sequence of states of equilibrium, represented by a curve on the bifurcation diagram, known as a branch of states of equilibrium. A nonlinear system often has multiple branches of states of equilibrium. In the bifurcation diagram, a bifurcation point is just a small part: a point at which two branches intersect. We illustrate our findings using bilayers of dissimilar materials (Fig. 1). Even for a bilayer with a critical strain for the onset of wrinkles much lower than that for the onset of creases, we find that a subcritical crease exists near the critical strain for the onset of wrinkles. We show that such a subcritical bifurcation can lead to channeling creases and snapping creases, at strains much below that for the onset of creases in a homogeneous material.

We analyze the critical conditions for the onset of wrinkles in bilayers by using the linear perturbation method (Sec. 2). We simulate the initiation and growth of creases by using the finite element method (Sec. 3). In particular, we use the Riks method to simulate subcritical creases. We construct a plane using the ratio of the elastic moduli and the ratio of thicknesses as coordinates. In this plane, the conditions of equal critical strains for the onset of wrinkles and creases form a curve. The curve, however, as mentioned above, does not demarcate whether wrinkles or creases will form. Rather, we show that bilayers of moduli and thicknesses near this boundary can have complex bifurcation diagrams, leading to, for example, bilayers to form creases even when the critical strain for the onset of wrinkles is much lower than that for the onset of creases (Sec. 4). Finally, we perform experiments to validate the different bifurcation behaviors (Sec. 5).

[1]Corresponding authors.

Contributed by the Applied Mechanics Division of ASME for publication in the Journal of Applied Mechanics. Manuscript received March 23, 2015; final manuscript received April 14, 2015; published online April 30, 2015. Editor: Yonggang Huang.

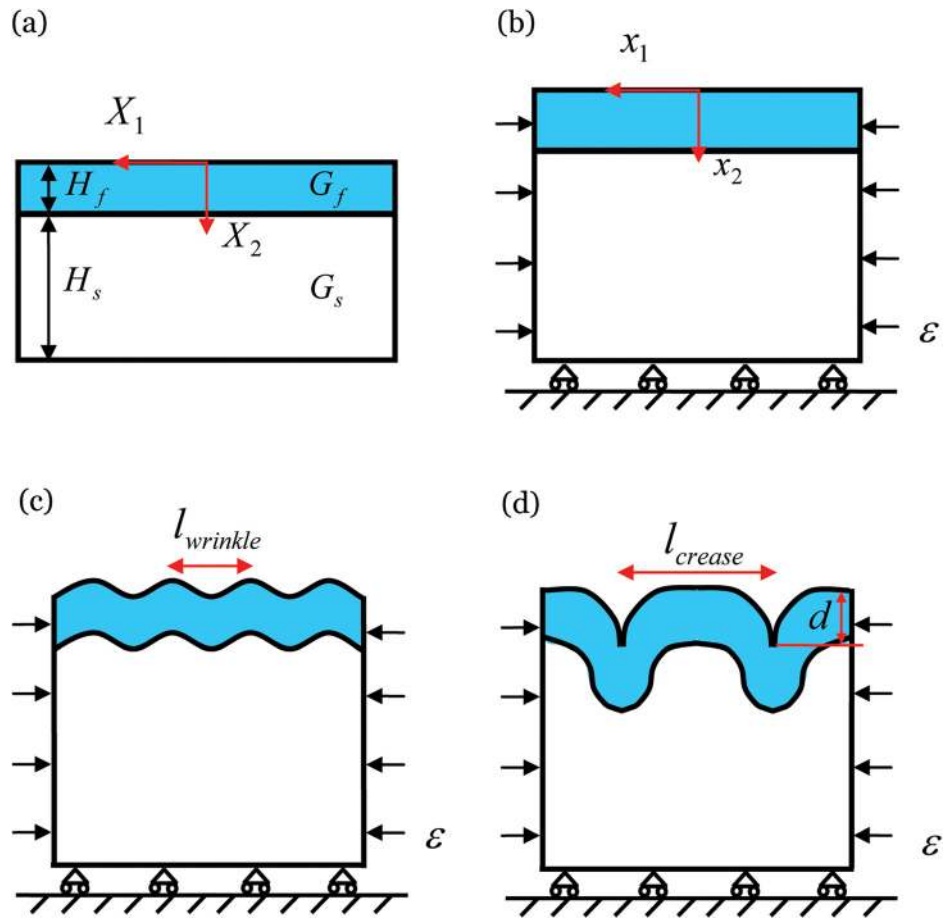

Fig. 1 A bilayer subject to compression may form wrinkles or creases. (*a*) A bilayer in the undeformed state. The surface of the film is set as $X_2 = 0$, and the axis of X_2 goes toward the substrate. (*b*) The bilayer subject to homogeneous compression. (*c*) The formation of wrinkles with wavelength $l_{wrinkle}$. (*d*) The formation of creases with spacing l_{crease}.

2 Linear Perturbation Analysis for Wrinkles

Consider a bilayer of a film and a substrate, with thicknesses H_f and H_s in the undeformed state (Fig. 1(*a*)). The two materials are taken to be neo-Hookean, with shear moduli G_f and G_s. Perfect bonding between the film and substrate is assumed. The bilayer is subject to homogeneous compression. The top of the film is traction-free. The bottom of the substrate is fixed in the vertical direction and is traction-free in the horizontal direction (Fig. 1(*b*)).

The onset of wrinkles corresponds to the existence of a nontrivial solution to the incremental boundary value problem, which is an eigenvalue problem. We formulate the governing equations and their incremental forms for a bilayer structure subject to an applied compression in Appendix A and solve the eigenvalue problem in Appendix B. Here, we describe the main results.

The eigenvalue problem Eq. (B7) gives the critical stretch $\lambda_1 = \lambda_c$ for wrinkle initiation under certain G_f/G_s, H_s/H_f, KH_f and a given state of strain λ_3, where K is the wave number in the reference state. As an example, we show the results of the uniaxial compression condition $\lambda_3 = 1/\sqrt{\lambda_1}$. The critical strain $\varepsilon_c = 1 - \lambda_c$ always decreases first and then increases as the nominal wavelength $L_{wrinkle}$ normalized by H_f increases, with $L_{wrinkle} = 2\pi/K$ (Fig. 2). Bending the film penalizes the modes with short wavelengths, while stretching the substrate penalizes the modes with long wavelengths. Thus, wrinkles with an intermediate wavelength $L^m_{wrinkle}$ can form under the lowest strain ε_m. When the film is very stiff and thin, like the case where a thin metal film is on the top of a thick polymeric substrate, ε_m can be smaller than 1%. Figure 7 shows ε_m and $L^m_{wrinkle}/H_f$ for different modulus ratio G_f/G_s and thickness ratio H_s/H_f under the uniaxial compression condition. In general, ε_m increases with the decrease of the modulus ratio G_f/G_s and the thickness ratio H_s/H_f.

We further notice that for an arbitrary constant λ_3, if we replace the variable λ_1 by $\lambda_1/\sqrt{\lambda_3}$ in the eigenvalue problem Eq. (B7) (Appendix B), the equation recovers the one under plane strain conditions with $\lambda_3 = 1$. This means that under generalized plane

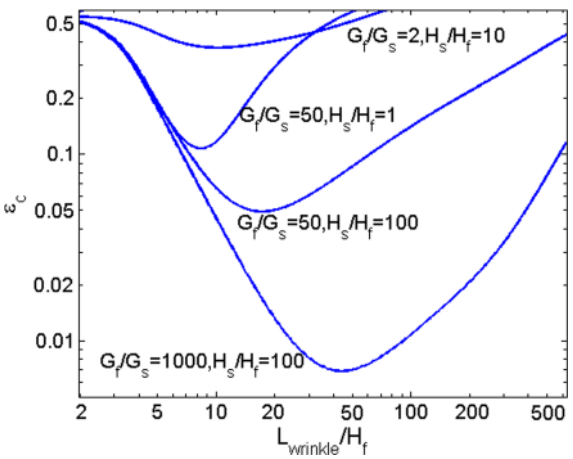

Fig. 2 The critical strain ε_c for the onset of wrinkles as a function of the wavelength for several ratios of shear moduli and thicknesses. For each curve, the critical strain reaches a minimum for wrinkles of certain wavelength.

strain conditions with an arbitrary λ_3, the critical strains, and thus the minimal strains, relates to the ones of plane strain conditions ε_c^{PE} and ε_m^{PE} by

$$1-\varepsilon_c^{PE}=\sqrt{\lambda_3}(1-\varepsilon_c) \text{ and } 1-\varepsilon_m^{PE}=\sqrt{\lambda_3}(1-\varepsilon_m) \quad (1)$$

and the wave number under the minimal strain K_m is independent of λ_3, although $k_m=K_m/\lambda_m$ depends on λ_3. A relation similar to Eq. (1) was also pointed out in Refs. [39,48,49].

Figures 3(*a*) and 3(*b*) show the contour plot of ε_m and $L^m_{wrinkle}/H_f$ in the plane with the axes of H_s/H_f and G_f/G_s. In Fig. 3(*a*), ε_m^{Uni} is the minimal strain under uniaxial compression conditions, while ε_m^{PE} is the corresponding value under plane strain conditions. When H_s/H_f and G_f/G_s are larger, ε_m is smaller. The line marked by "$\varepsilon_m^{Uni}=0.44$ and $\varepsilon_m^{PE}=0.35$" represents the conditions when the critical strain for the onset of creases coincides with that of wrinkles. Above this boundary of equal critical strain, the onset of wrinkles is under a strain smaller than the onset of creases for stiffer and thinner films. Below this boundary, the onset of wrinkles is under a strain larger than the onset of creases for more compliant and thicker films. Especially, when $G_f/G_s<1.65$, creases always form under a strain lower than wrinkles, no matter how large the thickness ratio H_s/H_f is. This was also predicted in Ref. [47] when the authors studied instability in a bilayer with infinite substrate, and this condition is close to the critical condition when wrinkles in a bilayer structure become unstable [45]. When H_s/H_f reaches around ten, with the further increase of H_s/H_f, the boundary of equal critical strain keeps flat, which means the thin film limit is reached. Since the critical condition of crease initiation under different loading conditions satisfies the same relation as the critical condition of wrinkle initiation, Eq. (1) [39], this boundary of equal critical strain is independent of loading condition. In Fig. 3(*b*), the nominal wavelengths $L^m_{wrinkle}/H_f$ are independent of the type of deformation. When H_s/H_f or G_f/G_s is larger, $L^m_{wrinkle}/H_f$ is larger.

3 Subcritical and Supercritical Creases

In a homogeneous material, creases are supercritical if they form under purely elastic compression and the bottom of the material is kept flat [39]. However, creases become subcritical if surface energy is large enough [50] or the material is free-standing [51]. Moreover, a bilayer with the same moduli of the film and substrate but a precompressed substrate can also form subcritical creases [52]. In this section, we use finite element method to study the initiation and growth of creases in a bilayer. We find that in a bilayer, creases can be either supercritical or subcritical.

We use the commercial finite element software ABAQUS to simulate the formation of creases. Both the film and substrate are taken to be incompressible neo-Hookean materials. We assume that creases form periodically, and the spacing between two neighboring creases is two times the total thickness of the film and substrate, which is similar to experimental observations [41,52]. Reflection symmetry of creases is assumed so that we only simulate half of a crease and the simulation box has the size of $(H_s+H_f)\times(H_s+H_f)$. Symmetry condition is prescribed on the left boundary, and the other three boundary conditions are applied as sketched in Fig. 1(*b*). We simulate the compression of the bilayer under plane strain conditions. Element type CPE4H is used. In order to break the translational symmetry of the surface, a defect with size as small as 10^{-3} of the film thickness is prescribed at the top left corner. Subcritical bifurcation is extremely defect sensitive [53], and this defect size is small enough so that its effect on the critical strain is negligible. On the other hand, to resolve the field close to the defect, mesh size around the defect is made much smaller than the defect size. In order to simulate subcritical creases, the static Riks method is implemented to solve the boundary value problem [54]. After the initiation of a crease, the crease tip folds up and forms self-contact. Because the combination of contact and the Riks method makes the convergence very difficult, a thick layer with extremely low shear modulus (1/200 of the film shear modulus) is added on the top of the film to prevent self-contact [52]. The top of the extremely compliant layer is confined to be flat so that instability only happens on the interface between the film and the compliant layer. As shown in Ref. [49], the interfacial crease asymptotically approaches the surface crease when the modulus of the compliant layer is much smaller than that of the film.

We simulate creases in bilayer structures for different ratios of moduli and thicknesses. We find that the creases can be subcritical or supercritical (Fig. 4(*a*)). Supercritical creases tend to form in a bilayer with thicker and more compliant film, while subcritical creases tend to form in a bilayer with thinner and stiffer film.

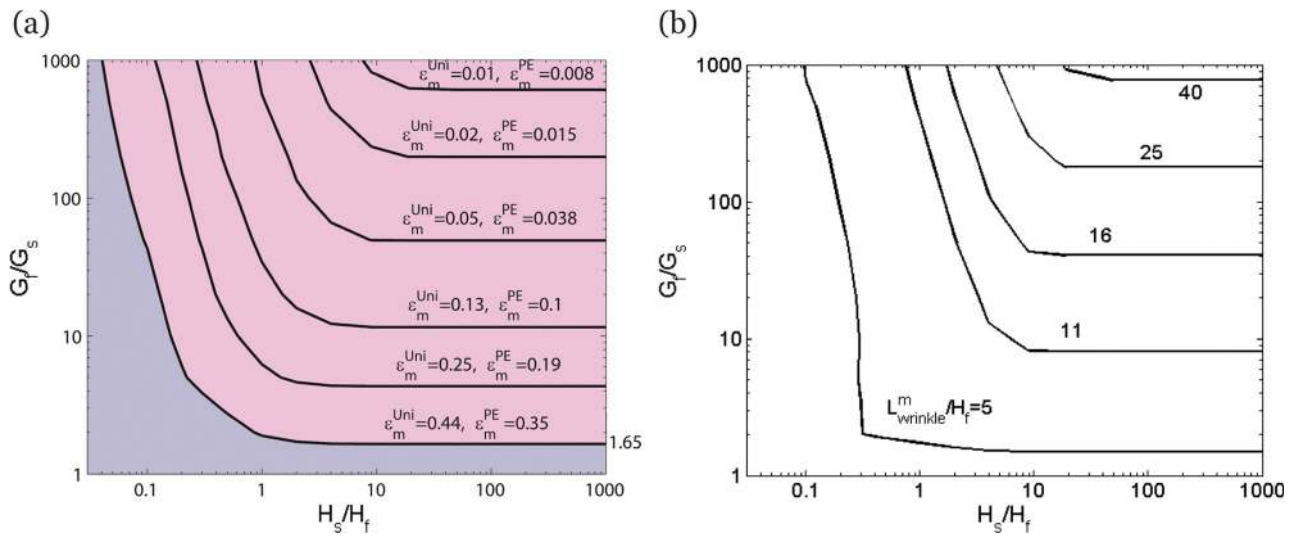

Fig. 3 The critical conditions for the onset of wrinkles represented in the plane with the axes of G_f/G_s and H_s/H_f. (*a*) The contour plots of the minimal critical strain under the uniaxial stress conditions or the plane strain conditions. The curve marked by $\varepsilon_m^{Uni}=0.44$ and $\varepsilon_m^{PE}=0.35$ represents the conditions when the critical strain for the onset of creases coincides with that of the onset of wrinkles. Above this curve, the critical strain for the onset of wrinkles is smaller than that of creases. Below this curve, the critical strain for the onset of wrinkles is larger than that of creases. (*b*) The corresponding nominal wavelengths are independent of the type of deformation.

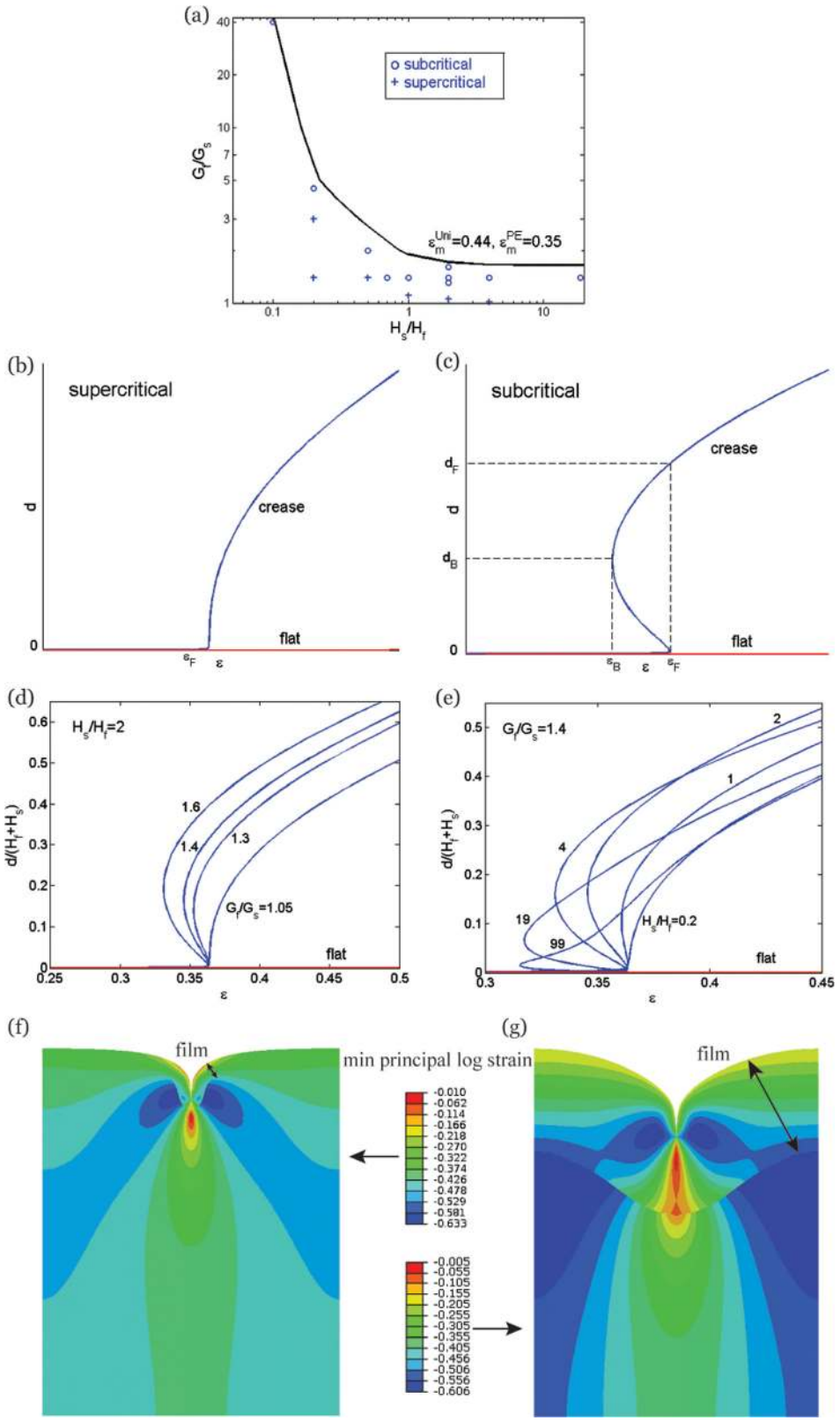

Fig. 4 The formation of creases in bilayers of various ratios of moduli and thicknesses. (*a*) Below the solid curve, the critical strain for the onset of wrinkles is larger than that of creases. Creases in a bilayer can be subcritical or supercritical. (*b*) Bifurcation diagram of a supercritical crease, where the applied strain represents the loading parameter, and the depth of the crease represents the state of the system. (*c*) Bifurcation diagram of a subcritical crease. (*d*) and (*e*) Calculated bifurcation diagrams for bilayers of some ratios of moduli and thicknesses. Morphology of subcritical creases right after snapping under the snapping forward strain $\varepsilon_F = 0.36$ for (*f*) $G_f/G_s = 1.4$ and $H_s/H_f = 19$ and (*g*) $G_f/G_s = 1.6$ and $H_s/H_f = 2$.

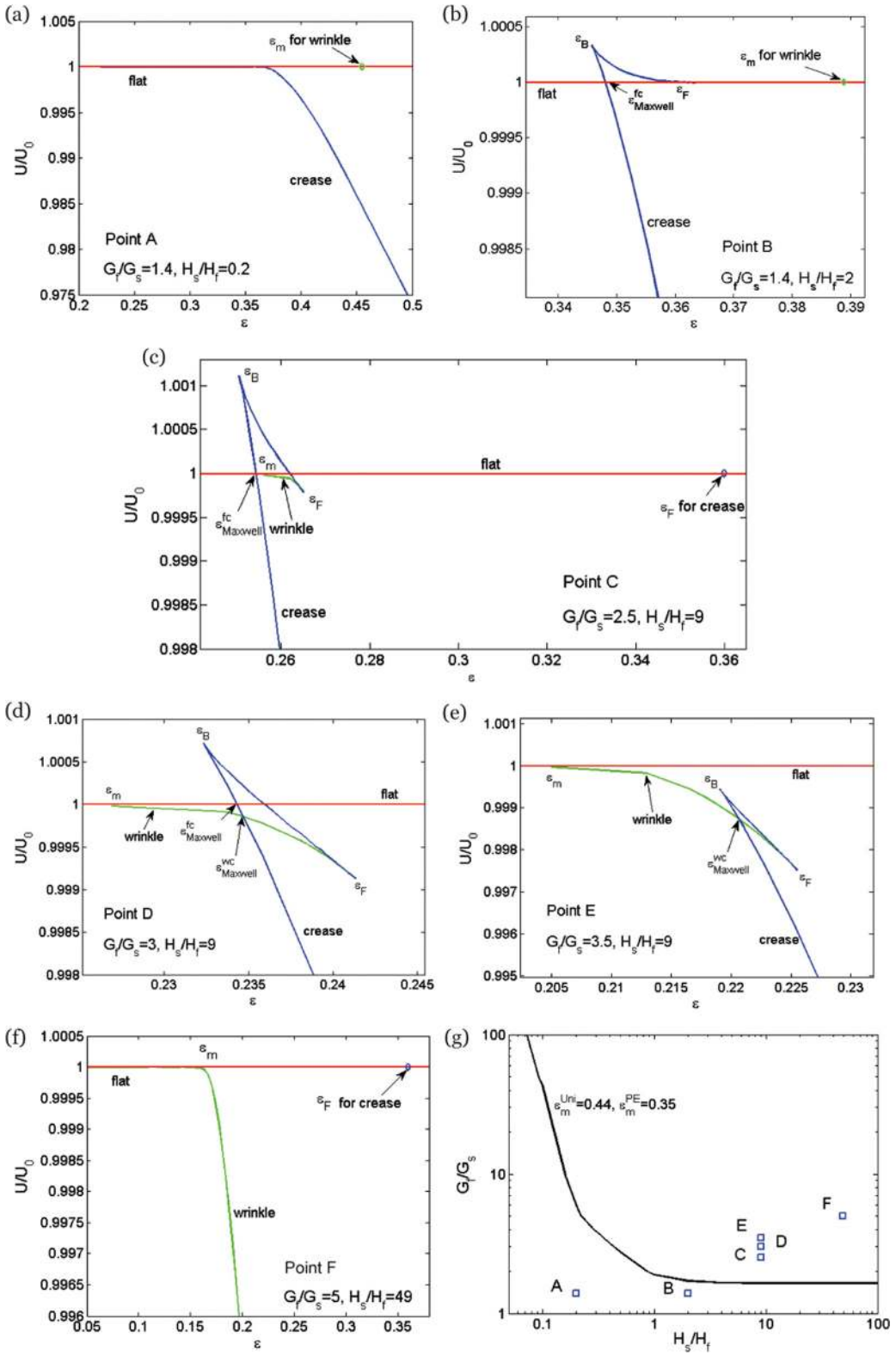

Fig. 5 Bilayers of various ratios of moduli and thicknesses exhibit various types of bifurcation. (*a*) and (*b*) The critical strain for the onset of creases is smaller than that for the onset of wrinkles. Point A: The creases are supercritical. Point B: The creases are subcritical and can coexist with the flat state at a strain smaller than the critical strain for the onset of creases. Such a strain for the coexistence of two states is known as Maxwell strain. (*c*)–(*f*) The critical strain for the onset of wrinkles is smaller than that for the onset of creases. Point C: The flat state and creases coexist at a strain $\varepsilon^{fc}_{Maxwell}$ even smaller than the critical strain for the onset of wrinkles. Point D: The wrinkles form at a certain strain and can coexist with the creases at a larger strain $\varepsilon^{wc}_{Maxwell}$. The creases can also coexist with the flat state at strain $\varepsilon^{fc}_{Maxwell}$. Point E: The wrinkles form at a certain strain and can coexist with the creases at a larger strain $\varepsilon^{wc}_{Maxwell}$. Point F: The wrinkles form, and no creases are found in the range of the strain calculated. (*g*) The points for various bifurcation behaviors identified on the plane of the axes G_f/G_s and H_s/H_f.

Figure 4(*b*) is a bifurcation diagram of a supercritical crease, where the applied strain represents the loading parameter, and the depth of the crease (defined in Fig. 1(*d*)) represents the state of the system. The flat state becomes unstable and creases initiate at strain 0.35 under plane strain conditions and 0.44 under uniaxial conditions. With further increase of strain, the crease gradually grows deeper (Fig. 4(*b*)). The curve marked by $G_f/G_s = 1.05$ in Fig. 4(*d*) and the curve marked by $H_s/H_f = 0.2$ in Fig. 4(*e*) show typical dependence of crease depth as a function of strain for supercritical creases under plane strain conditions. Here because of the existence of the extremely compliant layer, the critical strain for the initiation of creases ε_F is increased slightly to around 0.36.

Figure 4(*c*) is a bifurcation diagram of a subcritical crease. When the strain is smaller than the snapping backward strain ε_B, the flat state with $d = 0$ is the only solution to the boundary value problem. When the strain is larger than the snapping forward strain ε_F, the crease state with a finite depth is the only solution to the boundary value problem. When the strain is in between the snapping forward and snapping backward strains $\varepsilon_B < \varepsilon < \varepsilon_F$, both the flat state and the deep crease state are the solutions to the boundary value problem and can coexist. Figures 4(*d*) and 4(*e*) show the dependence of crease depth on external strain for subcritical creases under plain strain conditions. The snapping backward strain ε_B varies with H_s/H_f and G_f/G_s, while the snapping forward strain ε_F is a constant. The snapping forward happens when the critical strain of crease initiation is satisfied on the top of the film. Since the deformation in a bilayer structure is homogeneous before the initiation of creases, the snapping forward strain is 0.35 under plane strain conditions and 0.44 under uniaxial conditions. Morphology of subcritical creases under plane strain compression right after snapping at the snapping forward strain $\varepsilon_F = 0.36$ is shown for the case $G_f/G_s = 1.4$ and $H_s/H_f = 19$ (Fig. 4(*f*)), and for the case $G_f/G_s = 1.6$ and $H_s/H_f = 2$ (Fig. 4(*g*)), with color (shown online) representing the minimal principal logarithmic strain.

When $H_s/H_f = 2$, creases are supercritical if G_f/G_s is small enough (Fig. 4(*d*)). With the increase of G_f/G_s, the snapping backward strain for subcritical creases decreases, and therefore the hysteresis increases. The snapping forward and backward depths (d_F and d_B as defined in Fig. 4(*c*)) also increase with G_f/G_s. When $G_f/G_s = 1.4$, the depth-strain curve varies dramatically with H_s/H_f (Fig. 4(*e*)). When $H_s/H_f = 0.2$, the curve is monotonic, and the crease is supercritical. With the increase of H_s/H_f, creases become subcritical, and the hysteresis increases. However, the crease snapping forward and backward depths normalized by the total thickness $H_s + H_f$, $d/(H_s + H_f)$, increase and then decrease with the increase of H_s/H_f. We can see that when the critical condition of creases is lower than that of wrinkles, creases tend to be more supercritical for the points far away from the boundary of equal critical strain, i.e., for more compliant and thicker film. Moving closer to the boundary, i.e., for stiffer and thinner film, leads to more subcritical creasing behavior. In the subcritical region, when $G_f \gg G_s$ (for example, the point $H_s/H_f = 0.1$ and $G_f/G_s = 40$ in Fig. 4(*a*)), the thin and compliant substrate has negligible constraint to the film, and the bilayer approaches the limit of a free-standing homogeneous material [51].

4 Bifurcation Diagrams of Different Bifurcation Behaviors

It is tempting to expect that the boundary of the equal critical strain of wrinkles and creases demarcates regions in which wrinkles or creases form. However, in this section, we demonstrate remarkably rich bifurcation behavior when the ratios of moduli and thicknesses are different (Fig. 5). The simulations in this section are under plane strain conditions.

On the left of the equal critical strain curve, we find that the creases can be supercritical or subcritical (Fig. 4(*a*)). Figure 5(*a*) shows the computed bifurcation diagram for a supercritical crease with $G_f/G_s = 1.4$ and $H_s/H_f = 0.2$ (indicated as point A in Fig. 5(*g*)). In the bifurcation diagram, the applied strain ε represents the loading parameter, and the total elastic energy U normalized by the total elastic energy for the flat state U_0, U/U_0, represents the state of the system. The flat line $U/U_0 = 1$ represents the flat state. For a supercritical crease, U becomes smaller than U_0 after the formation of the crease. The minimal strain for the initiation of wrinkles ε_m (represented by the diamond in Fig. 5(*a*)) is higher than the critical strain for the initiation of creases. Figure 5(*b*) shows the bifurcation diagram of a subcritical crease with $G_f/G_s = 1.4$ and $H_s/H_f = 2$ (indicated as point B in Fig. 5(*g*)). The crease can coexist with the flat state at a strain smaller than the critical strain for the onset of creases. The strain of the coexistence is called the Maxwell strain $\varepsilon^{fc}_{Maxwell}$, defined as the critical condition when the energy of the deep crease state is the same as the flat state. The critical condition for the initiation of wrinkles ε_m, represented by the diamond, is also higher than the snapping forward strain ε_F.

When the critical strain for the onset of wrinkles ε_m is smaller than that for the onset of creases, creases instead of wrinkles may still form first, or wrinkles may further transit to creases under a strain much smaller than the critical strain for the onset of creases in a homogeneous material. Figure 5(*c*) is an example of this for $G_f/G_s = 2.5$ and $H_s/H_f = 9$ (indicated as point C in Fig. 5(*g*)). The line $U/U_0 = 1$ represents the flat state. The crease solution can coexist with the flat state under the Maxwell strain $\varepsilon^{fc}_{Maxwell}$, which is smaller than the critical strain for the onset of wrinkles ε_m. When the defect in the sample is small enough, the flat surface cannot overcome the energy barrier to form creases under $\varepsilon^{fc}_{Maxwell}$, but needs to go to a strain larger than $\varepsilon^{fc}_{Maxwell}$. Therefore, wrinkles may initiate at strain ε_m first, and then snap to creases under a larger strain. When the defect in the sample is large enough, creases can initiate directly from the flat surface, and channel through the sample. This explains why in Ref. [47] the authors observed creases experimentally under higher G_f/G_s than the value predicted by their theory, which only considers supercritical creases. The diamond in Fig. 5(*c*) represents the critical strain for the initiation of creases on the flat surface. We notice that the critical strain for the initiation of creases with the facilitation of wrinkles is much lower than the critical strain for the initiation of creases in a homogeneous material. Figure 5(*d*) shows the energy bifurcation diagram for $G_f/G_s = 3$ and $H_s/H_f = 9$ (indicated as point D in Fig. 5(*g*)). The flat surface forms wrinkles at strain ε_m, and the wrinkles can coexist with creases under a larger strain $\varepsilon^{wc}_{Maxwell}$, which is much smaller than the critical strain for the onset of creases in a homogeneous material (not indicated in the figure). On the other hand, creases can also coexist with the flat state under strain $\varepsilon^{fc}_{Maxwell}$, which satisfies $\varepsilon_m < \varepsilon^{fc}_{Maxwell} < \varepsilon^{wc}_{Maxwell}$. Figure 5(*e*) is the energy bifurcation diagram for $G_f/G_s = 3.5$ and $H_s/H_f = 9$ (indicated as point E in Fig. 5(*g*)). The crease solution no longer has an intersection with the flat state, but still has an intersection with the wrinkle solution. Wrinkles form on a flat surface at strain ε_m and can coexist with creases at a larger strain $\varepsilon^{wc}_{Maxwell}$, which is also much smaller than the critical strain for the onset of creases in a homogeneous material (not indicated in the figure). Figure 5(*f*) shows the energy bifurcation diagram for $G_f/G_s = 5$ and $H_s/H_f = 49$ (indicated as point F in Fig. 5(*g*)). The elastic energy U for the wrinkle solution becomes smaller than U_0 when the strain is larger than the critical strain for the onset of wrinkles ε_m. No other bifurcation is observed soon after the formation of wrinkles. The critical strain for the initiation of creases on a flat surface, represented by a diamond, is higher.

5 Experimental Results

The bifurcation behavior of supercritical creases (Fig. 5(*a*), point A) and wrinkles (Fig. 5(*f*), point F) is classical, whereas the other types of bifurcation diagrams are new. Here, experiments were conducted to realize these new behaviors, i.e., subcritical creases channeling from a flat surface (Fig. 6(*b*), corresponding to

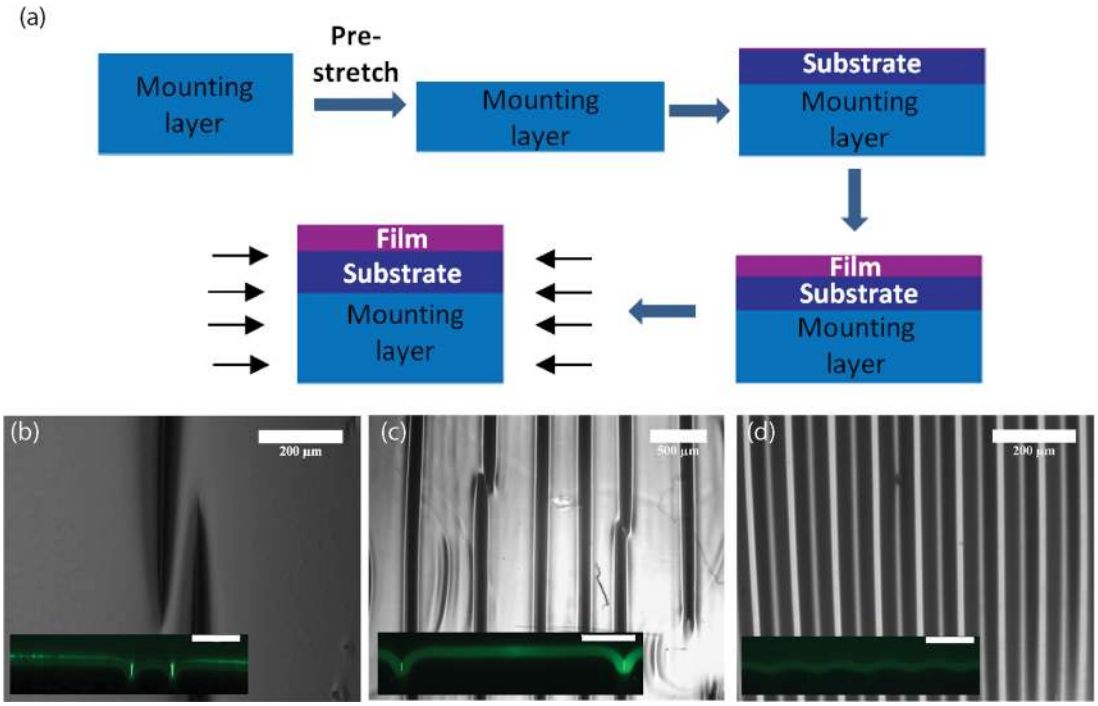

Fig. 6 Experimental setup and the observations of three types of bifurcation behavior. (*a*) A prestretched elastomeric mounting layer is used to apply compression to a film–substrate bilayer. Both the film and substrate are made of PDMS. We fabricate film–substrate bilayers of various modulus ratios to observe different types of bifurcation. (*b*), (*c*), and (*d*) the optical micrographs display the top views, and the inset confocal micrographs show the side views (the scale bars in the insets are equal to 100 μm). The micrographs are taken at the applied compressive strains where the instability first appear. (*b*) Subcritical creases at the strain of 0.37. (*c*) Coexistence of creases and wrinkles at the strain of 0.29. (*d*) Wrinkles at the strain of 0.21.

point B in Fig. 5(*b*)) and creases coexisting with wrinkles (Fig. 6(*c*), points C, D, and E in Figs. 5(*c*)–5(*e*)) in bilayers. The classical wrinkles were also realized as a comparison (Fig. 6(*d*)).

Uniform compression was applied to the bilayer structures through a prestretched mounting layer underneath the bilayers. The mounting layer needs to be stiff and thick enough so that it only functions to add a uniform compression to the bilayer and does not buckle. A schematic of the experiment procedure is shown in Fig. 6(*a*). The silica reinforced PDMS mounting layer with shear modulus 260 kPa and thickness 1 mm was prestretched uni-axially on a stretcher. Then, the substrate of the bilayer, a fully precured 30:1 (base to crosslinker ratio) PDMS layer (Sylgard 184, Dow Corning, Midland, MI) with thickness of approximately 550 μm was attached to the prestretched mounting layer using a thin layer (2–5 μm thick) of uncured PDMS with the same composition as the adhesive. The much thinner film (18–20 μm thick) was made by spin-coating uncured PDMS of various base:crosslinker compositions onto a trimethylchlorosiloxane treated glass slide at 4000 rpm for 90 s and then placing into a 120 °C oven for 10 min. The PDMS coated glass slide was attached to the substrate and the bilayer assembly was held at 40 °C for 16 hr to bond the layers and cure the film. By relaxing the prestretch of the mounting layer, uniaxial compression was applied to the film–substrate bilayer.

We realize the various types of bifurcation behavior in bilayers by changing the mass ratio of base to crosslinker, and therefore the modulus, of the film. The morphologies of channeling creases (Fig. 6(*b*)), wrinkles (Fig. 6(*d*)), and the coexistence of both (Fig. 6(*c*)) are contrasted using optical microscopy to visualize samples in top views. The substrate was 30:1 PDMS in all three cases but the film was progressively increased in modulus by using compositions of 15:1 in Fig. 6(*b*), 10:1 in Fig. 6(*c*), and 7.5:1 in Fig. 6(*d*). In Fig. 6(*b*), creases can clearly be recognized by their aperiodic spacings and sharp tips that resemble cracks. From a flat surface, the uni-axially compressed bilayer forms creases that channel across the surface at a critical strain of 0.37 (Video 1 in Appendix C). In contrast, classical wrinkles are formed spontaneously at a critical film strain between 0.18 and 0.21 (Fig. 6(*d*) and Video 3 in Appendix C). Wrinkles look quite periodic with alternating thicker and thinner lines, corresponding to peaks and troughs, respectively.

In Fig. 6(*c*), the image shows the coexistence of wrinkles and creases. The sample begins to develop wrinkles similar to those in Fig. 6(*d*) over the range of strains from 0.22 to 0.28 (apparently reflecting some variability in conditions across the sample surface, as well as some viscoelastic relaxation in the bilayer), but then at a strain of 0.28, creases form and channel across the surface (Video 2 in Appendix C), eventually causing the wrinkles to relax and disappear. This strain for the onset of creases is much less than that for channeling of subcritical or supercritical creases, in good agreement with simulations (Figs. 5(*c*)–5(*e*)).

Cross-sectional imaging of each sample was conducted using confocal microscopy. Fluorescein o-acrylate is added to show the films (in green in the online version). In the side view, wrinkles look quite smooth, while a crease forms a sharp tip and has a region of self-contact, highlighted by the brightness in color, which protrudes into the substrate. Delamination did not occur in any samples, as judged by the absence of localized upward deflection, which is characteristic of delamination.

6 Conclusions

In this paper, we study wrinkle and crease instability in bilayers and observe various types of bifurcation behavior. We study wrinkles in a bilayer with finite thickness of the substrate by the linear perturbation method. We simulate the initiation and growth of creases in bilayers by finite element method. The ratio of the elastic moduli and that of the thicknesses define a plane, and by

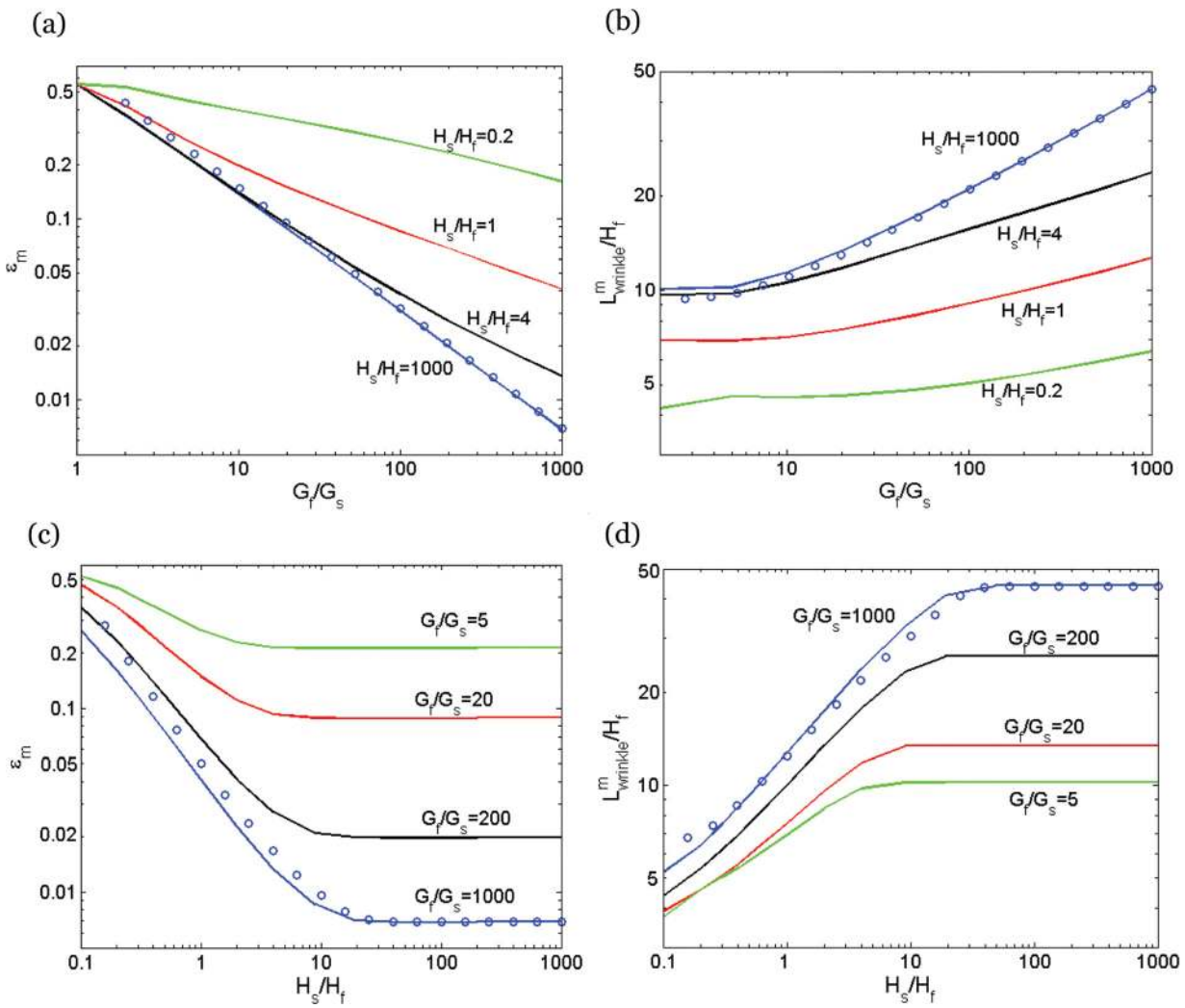

Fig. 7 The minimal critical strain ε_m and its corresponding wavelength $L^m_{wrinkle}/h_f$ depend on the ratios of moduli and thicknesses of the film and substrate. The solid curves are obtained when both the film and substrate are modeled as neo-Hookean materials. The circles correspond to approximate solutions when both the film and substrate are modeled as linearly elastic materials, and the film is modeled as a von Karman plate. The approximate solutions are accurate only when the film is much stiffer and thinner than the substrate.

comparing the onset conditions for wrinkles and creases, we find a curve of equal critical strain in that plane. Far below the curve when the critical strain for the onset of creases is much lower than that for the onset of wrinkles, the supercritical creases form. Right below the curve when the critical strain for the onset of creases is slightly lower than that for the onset of wrinkles, creases are subcritical and can channel into the bilayers at the Maxwell strain. Far above the equal critical strain curve, when the critical strain for the onset of wrinkles is much lower than that for the onset of creases, wrinkles form. Right above the curve, even when the critical strain for the onset of creases is higher than that for the onset of wrinkles, subcritical creases can still channel at the Maxwell strain, which could be much lower than the critical strain for the onset of creases in a homogeneous material. When the critical strain for the onset of wrinkles is lower than the channeling strain of creases, wrinkles form first, but a further compression can still cause channeling of creases from wrinkles. Experiments conducted on PDMS bilayers show different bifurcation behaviors under different ratios of moduli and thicknesses: wrinkles, channeling creases, and coexistence of wrinkles and creases.

Here, we demonstrate the significance to construct bifurcation diagrams to the study of instability. In this paper, we mainly focus on bilayers consisting of films and substrates of comparable elastic moduli. For bilayers consisting of stiff films on compliant substrates, rich secondary bifurcation after the formation of wrinkles, such as period doubling [55], ridge [48] and delamination [47], can happen. The similar way of construction of bifurcation diagrams can be applied to those studies.

Acknowledgment

The work at Harvard was supported by the NSF MRSEC (DMR 14-20570). The work at UMass was supported by NSF grant DMR-1309331, with additional support for AA through an NSF Graduate Research Fellowship (DGE-0907995).

Appendix A: Governing Equations and Their Incremental Forms

Here, we formulate the governing equations and their incremental forms of a bilayer subject to an applied compression. Choose the stress-free state before compression as the reference,

and name every material particle by its coordinate $\mathbf{X}$ in the reference state. After the deformation, each particle $\mathbf{X}$ moves to the current position $\mathbf{x}(\mathbf{X})$. The deformation gradient is defined as

$$F_{iK} = \frac{\partial x_i(\mathbf{X})}{\partial X_K} \tag{A1}$$

We model both layers of the bilayer structure as the incompressible neo-Hookean material with the free energy function

$$W(\mathbf{F}) = \frac{G}{2} F_{iK} F_{iK} - \pi(\det \mathbf{F} - 1) \tag{A2}$$

where G is the shear modulus, and $\pi(\mathbf{X})$ is the Lagrange multiplier to enforce the constraint of incompressibility $\det \mathbf{F} = 1$. The nominal stress $s_{iK} = \partial W(\mathbf{F})/\partial F_{iK}$ can be calculated as

$$s_{iK} = GF_{iK} - \pi H_{iK} \tag{A3}$$

where $\mathbf{H} = \mathbf{F}^{-\mathbf{T}}$. In equilibrium, the nominal stress satisfies that

$$\frac{\partial s_{iK}}{\partial X_K} = 0 \tag{A4}$$

inside the body. The boundary conditions are

$$s_{iK} N_K = 0 \tag{A5}$$

on the free surface of the film $X_2 = 0$ with N_K the normal direction of the surface in the reference state, and

$$s_{1K} N_K = 0 \text{ and } x_2 = X_2 \tag{A6}$$

on the bottom of the substrate $X_2 = H_\mathrm{f} + H_\mathrm{s}$. On the interface between the film and substrate $X_2 = H_\mathrm{f}$, the continuity of the traction and displacement needs to be satisfied

$$\left(s^\mathrm{f}_{iK} - s^\mathrm{s}_{iK}\right) N_K = 0 \text{ and } x^\mathrm{f}_i = x^\mathrm{s}_i \tag{A7}$$

where the superscripts f and s represent film and substrate respectively.

The above governing equations are perturbed in the current state with the independent variable $\mathbf{x}$, the coordinate in the current state. The displacement associated with the perturbation is written as $\mathbf{u}(\mathbf{x}) = \dot{\mathbf{x}}(\mathbf{X})$, and the perturbation of the deformation gradient becomes [56,57]

$$L_{ij}(\mathbf{x}) = \frac{\partial u_i(\mathbf{x})}{\partial x_j} = H_{jK} \dot{F}_{iK} \tag{A8}$$

The condition of incompressibility becomes [56,57]

$$L_{ii} = 0 \tag{A9}$$

Write the stress–stretch relation Eq. (A3) and the equilibrium Eq. (A4) in the incremental forms, and we get [56,57]

$$\dot{s}_{iK} F_{jK} = GF_{jK} F_{pK} L_{ip} + \pi L_{ji} - \dot{\pi} \delta_{ij} \tag{A10}$$

$$\frac{\partial \dot{s}_{iK} F_{jK}}{\partial x_j} = 0 \tag{A11}$$

The boundary conditions Eqs. (A5) and (A6) in the incremental form are

$$\dot{s}_{iK} F_{jK} n_j = 0 \tag{A12}$$

$$\dot{s}_{1K} F_{jK} n_j = 0 \text{ and } u_2 = 0 \tag{A13}$$

with n_j the normal direction of the surface in the current state, and the continuity condition Eq. (A7) becomes

$$\left(\dot{s}^\mathrm{f}_{iK} F^\mathrm{f}_{jK} - \dot{s}^\mathrm{s}_{iK} F^\mathrm{s}_{jK}\right) n_j = 0 \text{ and } u^\mathrm{f}_i = u^\mathrm{s}_i \tag{A14}$$

Governing Eqs. (A9)–(A11) together with the boundary conditions ((A12)–(A14)) constitute an incremental boundary value problem.

Appendix B: Linear Perturbation Analysis for Wrinkles

The onset of wrinkles corresponds to the existence of a nontrivial solution to the incremental boundary value problem, which is an eigenvalue problem.

Before the formation of wrinkles, the bilayer is subject to uniform compression in direction 1, with the deformation gradient $\mathbf{F} = \mathrm{diag}[\lambda_1, 1/\lambda_1\lambda_3, \lambda_3]$ in both the film and substrate, where the incompressibility has been imposed. The deformation in direction 3, λ_3, is determined by the boundary condition in direction 3. For example, for a plane strain condition $\lambda_3 = 1$, while for a uniaxial compression $\lambda_3 = 1/\sqrt{\lambda_1}$. Wrinkles are assumed to form parallel to direction 3 at a critical compression (Fig. 1(*c*)), with λ_3 intact. Separated solutions exist for the incremental boundary value problem with the perturbation in the following form:

$$\begin{cases} u_1 = f_1(x_2) \sin kx_1 \\ u_2 = f_2(x_2) \cos kx_1 \\ \dot{\pi} = f_3(x_2) \cos kx_1 \end{cases} \tag{B1}$$

where f_i $(i = 1, 2, 3)$ are three unknown functions, and k is the wave number in the current state, which relates the wave number in the reference state K by $k = K/\lambda_1$.

Insert Eq. (B1) into the equilibrium Eq. (A11) and the incompressibility condition (A9), with using the stress–stretch relation (A10). Three ordinary differential equations are obtained for the three unknown functions $f_i(x_2)$ $(i = 1, 2, 3)$. Eliminate f_1 and f_3, and we get a single equation for f_2.

$$\lambda_1^{-2}\lambda_3^{-2} f_2^{(4)} - \left(\lambda_1^2 + \lambda_1^{-2}\lambda_3^{-2}\right) k^2 f_2^{(2)} + k^4 \lambda_1^2 f_2 = 0 \tag{B2}$$

where $f_2^{(i)}$ means the ith derivative of f_2 with respect to x_2. The general solution to Eq. (B2) is

$$f_2^i(x_2) = A_i e^{kx_2} + B_i e^{-kx_2} + C_i e^{kx_2\lambda_1^2\lambda_3} + D_i e^{-kx_2\lambda_1^2\lambda_3} \tag{B3}$$

where $i = f, s$ corresponds to the solution in the film and substrate, and A_i, B_i, C_i, and D_i are eight unknown constants. f_1^i and f_3^i can be calculated correspondingly,

$$\begin{aligned} f_1^i(x_2) &= -A_i e^{kx_2} + B_i e^{-kx_2} - C_i \lambda_1^2 \lambda_3 e^{kx_2\lambda_1^2\lambda_3} + D_i \lambda_1^2 \lambda_3 e^{-kx_2\lambda_1^2\lambda_3}, \\ f_3^i(x_2) &= G_i k\left(\lambda_1^{-2}\lambda_3^{-2} - \lambda_1^2\right)\left(A_i e^{kx_2} - B_i e^{-kx_2}\right) \end{aligned} \tag{B4}$$

The eight boundary conditions (A12–A14) are

$$\begin{aligned} &\dot{s}^\mathrm{f}_{2K} F^\mathrm{f}_{2K} = 0 \text{ and } \dot{s}^\mathrm{f}_{1K} F^\mathrm{f}_{2K} = 0 \text{ at } x_2 = 0 \\ &\dot{s}^\mathrm{f}_{2K} F^\mathrm{f}_{2K} = \dot{s}^\mathrm{s}_{2K} F^\mathrm{s}_{2K}, \quad \dot{s}^\mathrm{f}_{1K} F^\mathrm{f}_{2K} = \dot{s}^\mathrm{s}_{1K} F^\mathrm{s}_{2K}, \quad u^\mathrm{f}_1 = u^\mathrm{s}_1, \text{ and} \\ &\quad u^\mathrm{f}_2 = u^\mathrm{s}_2 \text{ at } x_2 = H_\mathrm{f}/\lambda_1\lambda_3 \\ &\dot{s}^\mathrm{s}_{1K} F^\mathrm{s}_{2K} = 0 \text{ and } u^\mathrm{s}_2 = 0 \text{ at } x_2 = (H_\mathrm{f} + H_\mathrm{s})/\lambda_1\lambda_3 \end{aligned} \tag{B5}$$

Inserting Eqs. (B3) and (B4) into the eight boundary conditions (B5), we obtain eight linear algebraic equations for the eight unknown constants.

$$\mathbf{A}[A_f, B_f, C_f, D_f, A_s, B_s, C_s, D_s]^T = 0 \tag{B6}$$

where the 8×8 matrix $\mathbf{A}$ can be written as a function of dimensionless parameters G_f/G_s, H_s/H_f, KH_f, λ_1 and λ_3, $\mathbf{A} = \mathbf{A}(G_f/G_s, H_s/H_f, KH_f, \lambda_1, \lambda_3)$.

The existence of the a nontrivial solution to the incremental boundary value problem requires

$$\det \mathbf{A} = 0 \tag{B7}$$

The explicit expression of the matrix $\mathbf{A}$ is given as follows:

$$A_{11} = \lambda_1^2 + \lambda_1^{-2}\lambda_3^{-2}, \quad A_{12} = -\lambda_1^2 - \lambda_1^{-2}\lambda_3^{-2}, \quad A_{13} = 2/\lambda_3,$$
$$A_{14} = -2/\lambda_3, \quad A_{15} = A_{16} = A_{17} = A_{18} = 0 \tag{B8}$$

$$A_{21} = A_{22} = 2, \quad A_{23} = A_{24} = 1 + \lambda_1^4\lambda_3^2,$$
$$A_{25} = A_{26} = A_{27} = A_{28} = 0 \tag{B9}$$

$$A_{31} = \left(\lambda_1^2 + \lambda_1^{-2}\lambda_3^{-2}\right)e^{KH_f/\left(\lambda_1^2\lambda_3\right)}G_f/G_s,$$
$$A_{32} = -\left(\lambda_1^2 + \lambda_1^{-2}\lambda_3^{-2}\right)e^{-KH_f/\left(\lambda_1^2\lambda_3\right)}G_f/G_s,$$
$$A_{33} = 2e^{KH_f}G_f/(G_s\lambda_3), \quad A_{34} = -2e^{-KH_f}G_f/(G_s\lambda_3),$$
$$A_{35} = -\left(\lambda_1^2 + \lambda_1^{-2}\lambda_3^{-2}\right)e^{KH_f/\left(\lambda_1^2\lambda_3\right)},$$
$$A_{36} = \left(\lambda_1^2 + \lambda_1^{-2}\lambda_3^{-2}\right)e^{-KH_f/\left(\lambda_1^2\lambda_3\right)},$$
$$A_{37} = -2e^{KH_f}/\lambda_3, \quad A_{38} = 2e^{-KH_f}/\lambda_3 \tag{B10}$$

$$A_{41} = 2e^{KH_f/\left(\lambda_1^2\lambda_3\right)}G_f/G_s, \quad A_{42} = 2e^{-KH_f/\left(\lambda_1^2\lambda_3\right)}G_f/G_s,$$
$$A_{43} = \left(1 + \lambda_1^4\lambda_3^2\right)e^{KH_f}G_f/G_s,$$
$$A_{44} = \left(1 + \lambda_1^4\lambda_3^2\right)e^{-KH_f}G_f/G_s, \quad A_{45} = -2e^{KH_f/\left(\lambda_1^2\lambda_3\right)},$$
$$A_{46} = -2e^{-KH_f/\left(\lambda_1^2\lambda_3\right)}, \quad A_{47} = -\left(1 + \lambda_1^4\lambda_3^2\right)e^{KH_f}$$
$$A_{48} = -\left(1 + \lambda_1^4\lambda_3^2\right)e^{-KH_f} \tag{B11}$$

$$A_{51} = -A_{55} = -e^{KH_f/\left(\lambda_1^2\lambda_3\right)}, \quad A_{52} = -A_{56} = e^{-KH_f/\left(\lambda_1^2\lambda_3\right)},$$
$$A_{53} = -A_{57} = -e^{KH_f}\lambda_1^2\lambda_3, \quad A_{54} = -A_{58} = e^{-KH_f}\lambda_1^2\lambda_3 \tag{B12}$$

$$A_{61} = -A_{65} = e^{KH_f/\left(\lambda_1^2\lambda_3\right)}, \quad A_{62} = -A_{66} = e^{-KH_f/\left(\lambda_1^2\lambda_3\right)},$$
$$A_{63} = -A_{67} = e^{KH_f}, \quad A_{64} = -A_{68} = e^{-KH_f} \tag{B13}$$

$$A_{71} = A_{72} = A_{73} = A_{74} = 0, \quad A_{75} = 2e^{K(H_f+H_s)/\left(\lambda_1^2\lambda_3\right)},$$
$$A_{76} = 2e^{-K(H_f+H_s)/\left(\lambda_1^2\lambda_3\right)} \quad A_{77} = \left(1 + \lambda_1^4\lambda_3^2\right)e^{K(H_f+H_s)},$$
$$A_{78} = \left(1 + \lambda_1^4\lambda_3^2\right)e^{-K(H_f+H_s)}, \tag{B14}$$

$$A_{81} = A_{82} = A_{83} = A_{84} = 0, \quad A_{85} = e^{K(H_f+H_s)/\left(\lambda_1^2\lambda_3\right)},$$
$$A_{86} = e^{-K(H_f+H_s)/\left(\lambda_1^2\lambda_3\right)} \quad A_{87} = e^{K(H_f+H_s)}, \quad A_{88} = e^{-K(H_f+H_s)} \tag{B15}$$

By solving the eigenvalue problem Eq. (B7), we obtain the critical stretch $\lambda_1 = \lambda_c$, and therefore the critical strain $\varepsilon_c = 1 - \lambda_c$, for wrinkle initiation as a function of wave number KH_f. Minimization of ε_c with respect to KH_f gives the minimal critical strain ε_m and the corresponding wave length $L^m_{wrinkle}/H_f$, with $L_{wrinkle}$ defined as $L_{wrinkle} = 2\pi/K$.

Figure 7 shows ε_m and $L^m_{wrinkle}/H_f$ for different modulus ratios G_f/G_s and thickness ratios H_s/H_f under the uniaxial compression condition. For a fixed thickness ratio H_s/H_f, the minimal critical strain ε_m monotonically decreases with the increase of the modulus ratio G_f/G_s (Fig. 7(*a*)). When $G_f/G_s = 1$, the bilayer becomes one layer and ε_m reaches the Biot strain under the uniaxial compression condition 0.556 [26]. When the film is much stiffer and thinner than the substrate, a nonlinear theory modeling both the film and substrate as linear elastic materials and the film as a von Karman plate can predict the critical strain and wavelength of wrinkles reasonably well [27–29,34,58,59]. The critical strains obtained by the nonlinear theory for $H_s/H_f = 1000$ are plotted with blue circles for comparison [58]. When G_f/G_s is large, for instance $G_f/G_s = 1000$, the minimal critical strain ε_m for the nonlinear theory overlaps with the result for neo-Hookean material, because when H_s/H_f and G_f/G_s are both large, the critical strain is smaller than 1% and linear elasticity and the plate theory are applicable. When G_f/G_s is small, for instance $G_f/G_s = 2$, the assumption of linear elasticity overestimates ε_m for around 0.05. Under a fixed thickness ratio H_s/H_f, the nominal wavelength $L^m_{wrinkle}/H_f$ mostly increases with modulus ratio G_f/G_s (Fig. 7(*b*)). However, when $H_s/H_f = 0.2$, at around $G_f/G_s = 10$, $L^m_{wrinkle}/H_f$ increases, decreases and then increases again with G_f/G_s. This is due to two competing factors: with the increase of G_f/G_s, larger current wavelength becomes more energetically preferential, while the minimal strain ε_m decreases. Therefore, the nominal wavelength as the ratio of the current wavelength to the maximal stretch shows nonmonotonic dependence on G_f/G_s. Under fixed G_f/G_s, ε_m decreases with H_s/H_f (Fig. 7(*c*)), since it is easier to bend a thinner film. However, the nominal wavelength $L^m_{wrinkle}/H_f$ is smaller for smaller H_s/H_f (Fig. 7(*d*)), since a thin substrate strongly suppresses wrinkles with long wavelength. When H_s/H_f is large enough, both ε_m and $L^m_{wrinkle}/H_f$ reach a plateau and do not vary with the further increase of H_s/H_f, which represents the limiting case of a thin film on an infinitely thick substrate.

Appendix C: Supporting Information of Videos

Videos of the experiments can be found online.[1]

Video 1 shows the optical micrographs ($5\times$ objective lens) taken at one frame every 10 s, showing creases channeling across the surface at a film strain of 0.36. Three creases (black lines) channel toward the center of the sample along the direction perpendicular to the applied compression. The bilayer comprises a PDMS film with 15:1 (base:crosslinker) weight ratio and substrate with 30:1 ratio.

Video 2 shows the optical micrographs ($5\times$ objective lens) taken over a range of film strains from 0.08 to 0.28 showing the formation of wrinkles and subsequent channeling of creases across the surface. The surface remains in the flat state until a film strain of 0.22. At a film strain of 0.28, creases grow at the trough of the wrinkles and relax the wrinkles in-between. The bilayer comprises a 10:1 film and 30:1 substrate.

Video 3 shows the optical micrographs ($5\times$ objective lens) taken over a range of film strains from 0.02 to 0.21 showing the formation of wrinkles. Faint wrinkles begin to appear at a film strain of 0.18 and continue to grow with additional compression. The film is 7.5:1 and the substrate is 30:1.

References

[1] Genzer, J., and Groenewold, J., 2006, "Soft Matter With Hard Skin: From Skin Wrinkles to Templating and Material Characterization," Soft Matter, **2**(4), pp. 310–323.

[2] Chen, X., and Yin, J., 2010, "Buckling Patterns of Thin Films on Curved Compliant Substrates With Applications to Morphogenesis and Three-Dimensional Micro-Fabrication," Soft Matter, **6**(22), pp. 5667–5680.

[3] Li, B., Cao, Y. P., Feng, X. Q., and Gao, H. J., 2012, "Mechanics of Morphological Instabilities and Surface Wrinkling in Soft Materials: A Review," Soft Matter, **8**(21), pp. 5728–5745.

[4] Khang, D. Y., Jiang, H. Q., Huang, Y., and Rogers, J. A., 2006, "A Stretchable Form of Single-Crystal Silicon for High-Performance Electronics on Rubber Substrates," Science, **311**(5758), pp. 208–212.

[1] https://www.youtube.com/channel/UCNvmQTlZ_xMSYgZ8q1qLvPQ/videos

[5] Stafford, C. M., Harrison, C., Beers, K. L., Karim, A., Amis, E. J., Vanlandingham, M. R., Kim, H. C., Volksen, W., Miller, R. D., and Simonyi, E. E., 2004, "A Buckling-Based Metrology for Measuring the Elastic Moduli of Polymeric Thin Films," Nat. Mater., **3**(8), pp. 545–550.
[6] Lin, P. C., Vajpayee, S., Jagota, A., Hui, C. Y., and Yang, S., 2008, "Mechanically Tunable Dry Adhesive From Wrinkled Elastomers," Soft Matter, **4**(9), pp. 1830–1835.
[7] Chan, E. P., Smith, E. J., Hayward, R. C., and Crosby, A. J., 2008, "Surface Wrinkles for Smart Adhesion," Adv. Mater., **20**(4), pp. 711–716.
[8] Lin, P. C., and Yang, S., 2009, "Mechanically Switchable Wetting on Wrinkled Elastomers With Dual-Scale Roughness," Soft Matter, **5**(5), pp. 1011–1018.
[9] Kim, J., Yoon, J., and Hayward, R. C., 2010, "Dynamic Display of Biomolecular Patterns Through an Elastic Creasing Instability of Stimuli-Responsive Hydrogels," Nat. Mater., **9**(2), pp. 159–164.
[10] Kucken, M., and Newell, A. C., 2004, "A Model for Fingerprint Formation," Europhys. Lett., **68**(1), pp. 141–146.
[11] Pauchard, L., and Couder, Y., 2004, "Invagination During the Collapse of an Inhomogeneous Spheroidal Shell," Europhys. Lett., **66**(5), pp. 667–673.
[12] Savin, T., Kurpios, N. A., Shyer, A. E., Florescu, P., Liang, H. Y., Mahadevan, L., and Tabin, C. J., 2011, "On the Growth and Form of the Gut," Nature, **476**(7358), pp. 57–62.
[13] Richman, D. P., Stewart, R. M., Hutchinson, J. W., and Caviness, V. S., 1975, "Mechanical Model of Brain Convolutional Development," Science, **189**(4196), pp. 18–21.
[14] Bayly, P. V., Taber, L. A., and Kroenke, C. D., 2014, "Mechanical Forces in Cerebral Cortical Folding: A Review of Measurements and Models," J. Mech. Behav. Biomed. Mater., **29**(S), pp. 568–581.
[15] Budday, S., Raybaud, C., and Kuhl, E., 2014, "A Mechanical Model Predicts Morphological Abnormalities in the Developing Human Brain," Sci. Rep., **4**, p. 5644.
[16] Lidmar, J., Mirny, L., and Nelson, D. R., 2003, "Virus Shapes and Buckling Transitions in Spherical Shells," Phys. Rev. E, **68**(5), p. 051910.
[17] Dumais, J., and Steele, C. R., 2000, "New Evidence for the Role of Mechanical Forces in the Shoot Apical Meristem," J. Plant Growth Regul., **19**(1), pp. 7–18.
[18] Liang, H. Y., and Mahadevan, L., 2009, "The Shape of a Long Leaf," Proc. Natl. Acad. Sci. U.S.A., **106**(52), pp. 22049–22054.
[19] Liang, H. Y., and Mahadevan, L., 2011, "Growth, Geometry, and Mechanics of a Blooming Lily," Proc. Natl. Acad. Sci. U.S.A., **108**(14), pp. 5516–5521.
[20] Armon, S., Efrati, E., Kupferman, R., and Sharon, E., 2011, "Geometry and Mechanics in the Opening of Chiral Seed Pods," Science, **333**(6050), pp. 1726–1730.
[21] Shipman, P. D., and Newell, A. C., 2004, "Phyllotactic Patterns on Plants," Phys. Rev. Lett., **92**(16), p. 168102.
[22] Dervaux, J., and Amar, M. B., 2008, "Morphogenesis of Growing Soft Tissues," Phys. Rev. Lett., **101**(6), p. 068101.
[23] Katifori, E., Alben, S., Cerda, E., Nelson, D. R., and Dumais, J., 2010, "Foldable Structures and the Natural Design of Pollen Grains," Proc. Natl. Acad. Sci. U.S.A., **107**(17), pp. 7635–7639.
[24] Yin, J., Cao, Z. X., Li, C. R., Sheinman, I., and Chen, X., 2008, "Stress-Driven Buckling Patterns in Spheroidal Core/Shell Structures," Proc. Natl. Acad. Sci. U.S.A., **105**(49), pp. 19132–19135.
[25] Hohlfeld, E., and Mahadevan, L., 2011, "Unfolding the Sulcus," Phys. Rev. Lett., **106**(10), p. 105702.
[26] Biot, M. A., 1963, "Surface Instability of Rubber in Compression," Appl. Sci. Res., **12**(2), pp. 168–182.
[27] Chen, X., and Hutchinson, J. W., 2004, "Herringbone Buckling Patterns of Compressed Thin Films on Compliant Substrates," ASME J. Appl. Mech., **71**(5), pp. 597–603.
[28] Audoly, B., and Boudaoud, A., 2008, "Buckling of a Stiff Film Bound to a Compliant Substrate—Part I: Formulation, Linear Stability of Cylindrical Patterns, Secondary Bifurcations," J. Mech. Phys. Solids, **56**(7), pp. 2401–2421.
[29] Song, J., Jiang, H., Liu, Z. J., Khang, D. Y., Huang, Y., Rogers, J. A., Lu, C., and Koh, C. G., 2008, "Buckling of a Stiff Thin Film on a Compliant Substrate in Large Deformation," Int. J. Solids Struct., **45**(10), pp. 3107–3121.
[30] Kim, D. H., Lu, N. S., Ma, R., Kim, Y. S., Kim, R. H., Wang, S. D., Wu, J., Won, S. M., Tao, H., Islam, A., Yu, K. J., Kim, T. I., Chowdhury, R., Ying, M., Xu, L. Z., Li, M., Chung, H. J., Keum, H., McCormick, M., Liu, P., Zhang, Y. W., Omenetto, F. G., Huang, Y. G., Coleman, T., and Rogers, J. A., 2011, "Epidermal Electronics," Science, **333**(6044), pp. 838–843.
[31] Keplinger, C., Sun, J. Y., Foo, C. C., Rothemund, P., Whitesides, G. M., and Suo, Z. G., 2013, "Stretchable, Transparent, Ionic Conductors," Science, **341**(6149), pp. 984–987.
[32] Kolle, M., Lethbridge, A., Kreysing, M., Baumberg, J. J., Aizenberg, J., and Vukusic, P., 2013, "Bio-Inspired Band-Gap Tunable Elastic Optical Multilayer Fibers," Adv. Mater., **25**(15), pp. 2239–2245.
[33] Bowden, N., Brittain, S., Evans, A. G., Hutchinson, J. W., and Whitesides, G. M., 1998, "Spontaneous Formation of Ordered Structures in Thin Films of Metals Supported on an Elastomeric Polymer," Nature, **393**(6681), pp. 146–149.
[34] Cerda, E., and Mahadevan, L., 2003, "Geometry and Physics of Wrinkling," Phys. Rev. Lett., **90**(7), p. 074302.
[35] Tanaka, T., Sun, S. T., Hirokawa, Y., Katayama, S., Kucera, J., Hirose, Y., and Amiya, T., 1987, "Mechanical Instability of Gels at the Phase-Transition," Nature, **325**(6107), pp. 796–798.
[36] Gent, A. N., and Cho, I. S., 1999, "Surface Instabilities in Compressed or Bent Rubber Blocks," Rubber Chem. Technol., **72**(2), pp. 253–262.
[37] Ghatak, A., and Das, A. L., 2007, "Kink Instability of a Highly Deformable Elastic Cylinder," Phys. Rev. Lett., **99**(7), p. 076101.
[38] Trujillo, V., Kim, J., and Hayward, R. C., 2008, "Creasing Instability of Surface-Attached Hydrogels," Soft Matter, **4**(3), pp. 564–569.
[39] Hong, W., Zhao, X. H., and Suo, Z. G., 2009, "Formation of Creases on the Surfaces of Elastomers and Gels," Appl. Phys. Lett., **95**(11), p. 111901.
[40] Wang, Q. M., Zhang, L., and Zhao, X. H., 2011, "Creasing to Cratering Instability in Polymers Under Ultrahigh Electric Fields," Phys. Rev. Lett., **106**(11), p. 118301.
[41] Cai, S. Q., Chen, D. Y., Suo, Z. G., and Hayward, R. C., 2012, "Creasing Instability of Elastomer Films," Soft Matter, **8**(5), pp. 1301–1304.
[42] Weiss, F., Cai, S., Hu, Y., Kang, M. K., Huang, R., and Suo, Z., 2013, "Creases and Wrinkles on the Surface of a Swollen Gel," J. Appl. Phys., **114**(7), p. 073507.
[43] Dervaux, J., Couder, Y., Guedeau-Boudeville, M. A., and Amar, M. B., 2011, "Shape Transition in Artificial Tumors: From Smooth Buckles to Singular Creases," Phys. Rev. Lett., **107**(1), p. 018103.
[44] Diab, M. Z., Zhang, T., Zhao, R. K., Gao, H. J., and Kim, K. S., 2013, "Ruga Mechanics of Creasing: From Instantaneous to Setback Creases," Proc. R. Soc. London, Ser. A, **469**(2157), p. 20120753.
[45] Hutchinson, J. W., 2013, "The Role of Nonlinear Substrate Elasticity in the Wrinkling of Thin Films," Philos. Trans. R. Soc., A, **371**(1993), p. 20120422.
[46] Wu, Z., Bouklas, N., and Huang, R., 2013, "Swell-Induced Surface Instability of Hydrogel Layers With Material Properties Varying in Thickness Direction," Int. J. Solids Struct., **50**(3–4), pp. 578–587.
[47] Wang, Q. M., and Zhao, X. H., 2014, "Phase Diagrams of Instabilities in Compressed Film-Substrate Systems," ASME J. Appl. Mech., **81**(5), p. 051004.
[48] Cao, Y. P., and Hutchinson, J. W., 2012, "Wrinkling Phenomena in Neo-Hookean Film/Substrate Bilayers," ASME J. Appl. Mech., **79**(3), p. 031019.
[49] Jin, L., Chen, D., Hayward, R. C., and Suo, Z., 2014, "Creases on the Interface Between Two Soft Materials," Soft Matter, **10**(2), pp. 303–311.
[50] Chen, D. Y., Cai, S. Q., Suo, Z. G., and Hayward, R. C., 2012, "Surface Energy as a Barrier to Creasing of Elastomer Films: An Elastic Analogy to Classical Nucleation," Phys. Rev. Lett., **109**(3), p. 038001.
[51] Hohlfeld, E., and Mahadevan, L., 2012, "Scale and Nature of Sulcification Patterns," Phys. Rev. Lett., **109**(2), p. 025701.
[52] Chen, D., Jin, L., Suo, Z., and Hayward, R. C., 2014, "Controlled Formation and Disappearance of Creases," Mater. Horiz., **1**(2), pp. 207–213.
[53] Jin, L., Takei, A., and Hutchinson, J. W., "Mechanics of Wrinkle/Ridge Transitions in Thin Film/Substrate Systems," J. Mech. Phys. Solids (submitted).
[54] Riks, E., 1972, "The Application of Newton's Method to the Problem of Elastic Stability," ASME J. Appl. Mech., **39**(4), p. 1060.
[55] Pocivavsek, L., Dellsy, R., Kern, A., Johnson, S., Lin, B. H., Lee, K. Y. C., and Cerda, E., 2008, "Stress and Fold Localization in Thin Elastic Membranes," Science, **320**(5878), pp. 912–916.
[56] Cai, S. Q., Bertoldi, K., Wang, H. M., and Suo, Z. G., 2010, "Osmotic Collapse of a Void in an Elastomer: Breathing, Buckling and Creasing," Soft Matter, **6**(22), pp. 5770–5777.
[57] Ogden, R. W., 1997, *Non-Linear Elastic Deformation*, Dover Publications, New York.
[58] Huang, Z. Y., Hong, W., and Suo, Z., 2005, "Nonlinear Analyses of Wrinkles in a Film Bonded to a Compliant Substrate," J. Mech. Phys. Solids, **53**(9), pp. 2101–2118.
[59] Jiang, H. Q., Khang, D. Y., Song, J. Z., Sun, Y. G., Huang, Y. G., and Rogers, J. A., 2007, "Finite Deformation Mechanics in Buckled Thin Films on Compliant Supports," Proc. Natl. Acad. Sci. U.S.A., **104**(40), pp. 15607–15612.